Electron Photodetachment from Aqueous Anions. 3. Dynamics of Geminate Pairs Derived from Photoexcitation of Mono- vs Polyatomic Anions†

Rui Lian, Dmitri A. Oulianov, Robert A. Crowell, and Ilya A. Shkrob*

Chemistry Division, Argonne National Laboratory, Argonne, Illinois 60439

Xiyi Chen and Stephen E. Bradforth

Department of Chemistry, University of Southern California, Los Angeles, California 90089

Received: February 16, 2006; In Final Form: May 22, 2006

Photostimulated electron detachment from aqueous inorganic anions is the simplest example of solvent-mediated electron transfer reaction. As such, this photoreaction became the subject of many ultrafast studies. Most of these studied focused on the behavior of halide anions, in particular, iodide, that is readily accessible in the UV. In this study, we contrast the behavior of these halide anions with that of small polyatomic anions, such as pseudohalide anions (e.g., HS^-) and common polyvalent anions (e.g., SO_3^{2-}). Geminate recombination dynamics of hydrated electrons generated by 200 nm photoexcitation of aqueous anions (I^-, Br^-, OH^-, HS^-, CNS^-, CO_3^{2-}, SO_3^{2-}, and $Fe(CN)_6^{4-}$) have been studied. Prompt quantum yields for the formation of solvated, thermalized electrons and quantum yields for free electrons were determined. Pump−probe kinetics for 200 nm photoexcitation were compared with kinetics obtained at lower photoexcitation energy (225 or 242 nm) for the same anions, where possible. Free diffusion and mean force potential models of geminate recombination dynamics were used to analyze these kinetics. These analyses suggest that for polyatomic anions (including all polyvalent anions studied) the initial electron distribution has a broad component, even at relatively low photoexcitation energy. There seems to be no well-defined threshold energy below which the broadening of this electron distribution does not occur, as is the case for halide anions. The constancy of (near-unity) prompt quantum yields vs the excitation energy as the latter is scanned across the lowest charge-transfer-to-solvent band of the anion is observed for halide anions but not for other anions: the prompt quantum yields are considerably less than unity and depend strongly on the excitation energy. Our study suggests that halide anions are in the class of their own; electron photodetachment from polyatomic, especially polyvalent, anions exhibits qualitatively different behavior.

1. Introduction

In part 1 of this series,[1] terminal quantum yields for hydrated electron generated by photoinduced electron detachment from various aqueous anions have been determined. Most of these anions exhibit the distinctive charge-transfer-to-solvent (CTTS) band in their UV absorption spectra that implicated the involvement of a short-lived excited state (CTTS state) mediating electron photodetachment.[2,3] Following the dissociation of this CTTS state, a geminate pair of the electron and the residual radical (such as hydroxyl for HO^- and iodine atom for I^-) is formed in less than 200 fs. Some of these geminate pairs recombine (typically, within 0.1−1 ns), while the rest escape to the solvent bulk, yielding "free" electrons and radicals that undergo slow recombination and other secondary reactions.[4−11] The electron yields given by Sauer et al.[1] are those for *free* electrons that escaped recombination with their geminate partners at $t \rightarrow \infty$ (i.e., the terminal quantum yield ϕ_∞ attained at the end of the time interval that is much longer than the time scale of the geminate kinetics for an isolated pair). Such results per se are of limited import for understanding the photophysics of electron detachment in solution because this yield is a product of the prompt quantum yield ϕ_0 for electron formation and the survival probability Ω_∞ of the resulting geminate pair.[1,4,10] The latter parameter can be determined by time-resolved measurement on a subnanosecond time scale. For many aqueous anions, such a measurement requires a pulsed source of ultraviolet (UV) or vacuum UV light,[2] and ultrafast pump−probe studies of these photosystems has only recently become possible.

This study pursued three objectives: (i) to extend previous observations of electron dynamics in photoexcited halide anions[4−6] and hydroxide[10] to other common CTTS anions, including polyvalent ones, (ii) to find the effect of the photon energy on these electron dynamics (extending our detailed study of iodide[6] to other anions); and (iii) to determine the prompt quantum yield ϕ_0 for several classes of aqueous anions. Importantly, we limit ourselves to *one-photon* excitation of these anions. Because of different selection rules, the photophysics of biphotonic excitation is different from that of monophotonic excitation (e.g., ref 10).

To achieve these goals, recombination dynamics of hydrated electrons (e_{aq}^-) generated by 200 nm photoexcitation of several aqueous anions were observed and these kinetic data and photo- and actino- metric measurements were used to obtain *directly* the prompt quantum yield for the formation of thermalized electrons. Previously, such yields had been estimated for two halide anions only, I^- and Br^-, and were found to be unity

* To whom correspondence should be addressed. Telephone: 630-252-9516. Fax: 630-252-4993. E-mail: shkrob@anl.gov.

† Work performed under the auspices of the Office of Science, Division of Chemical Science, US-DOE, under Contract No. W-31-109-ENG-38.

10.1021/jp0610113 CCC: $33.50
Published on Web 07/04/2006

across their lower energy CTTS subband.[4,12] In this work, we present a larger pattern of these quantum yields. Our results suggest that polyatomic anions generally have ϕ_0 substantially lower than unity. Furthermore, for some nonhalide anions, ϕ_0 systematically increases with the excitation energy from the very onset of the CTTS band.

The geminate recombination kinetics obtained for 200 nm photoexcitation of several aqueous anions were compared with pump−probe kinetics obtained for the same anions at lower photoexcitation energy (242 or 225 nm). Two models of geminate recombination in the CTTS photosystems, the free diffusion model[13] and the mean force potential (MFP) model, [4,10,11] were used to analyze these data sets. This analysis suggests that *for aqueous anions other than halides and simple pseudohalides (such as OH^- and HS^-), the initial spatial distribution of photogenerated electrons has a broad component, regardless of the photoexcitation energy*. These results generalize our observations for aqueous I^- [4,6] and observations of Barthel and Schwartz for Na^- in ethers.[8] The narrow component in this distribution originates from the dissociation of the precursor CTTS state which proceeds through a succession of localized electron states. Such a picture has been suggested and corroborated by quantum molecular dynamics calculations carried out by several research groups.[14,15,16] It is not clear from our kinetic data whether this type of a photoprocess occurs for polyvalent anions at all—and possibly for some polyatomic monovalent anions, such as CSN^-.

Direct promotion of the electron from a photoexcited anion to the conduction band of the solvent is a possible cause for the occurrence of the *broad component* in the electron distribution at higher photon energy. It is well-known that in photoionization of solvent and/or neutral solute molecules in polar and nonpolar liquids, the width of the electron distribution increases with the photoexcitation energy (e.g., ref 17). This trend can be accounted for by a longer thermalization path for the conduction band electrons (emitted in the course of the direct ionization) as their kinetic energy increases. Electron photodetachment from aqueous halide anions broadly conforms to the behavior expected for this photoionization mechanism: there is a threshold energy for the electron distribution broadening (corresponding to the onset of electron promotion to the conduction band) and systematic increase in the width of the electron distribution with the total energy of photoexcitation, as observed by Bradforth and co-workers.[6]

In other cases (e.g., in low energy photoionization of water), [18,19] different mechanisms are in play. Indeed, the energetics of this photoionization are such that it cannot involve these conduction band electrons; yet the resulting electron distribution is quite broad (ca. 1 nm width). Many theories of this low energy photoprocess have been suggested (see ref 19 for a brief review). The current favorite is rapid electron transfer from photoexcited water molecule to a "pre-existing" trap in the solvent bulk (this reaction is thought to be concerted with ultrafast deprotonation of the resulting hole).[20] Our results for photo-CTTS reactions of aqueous polyatomic anions suggest that a similar photoprocess may occur in the course of electron photodetachment from such anions: there appears to exist for at least two monovalent anions a relatively broad initial electron distribution without the involvement of the conduction band of the solvent.

2. Experimental Section

200 nm Photoexcitation. The pico- and femtosecond kinetic measurements reported below were obtained using a 1 kHz Ti:sapphire setup, details of which are given in ref 10. This setup provided 60 fs fwhm, 3 mJ light pulses centered at 800 nm. One part of the beam was used to generate 800 nm probe pulses while the other part was used to generate the 200 nm (fourth harmonic) pump pulses. Up to 20 μJ of the 200 nm light was produced this way (300−350 fs fwhm pulse). The pump and probe beams were perpendicularly polarized and overlapped at the surface of a 150 μm thick high-speed jet at 6.5°. Typically, 150−200 delay time points acquired on a quasi-logarithmic grid were used to obtain the decay kinetics of the electron out to 600 ps. The vertical bars in the figures represent 95% confidence limits for each data point. The details of the detection and the flow system are given elsewhere.[10,11]

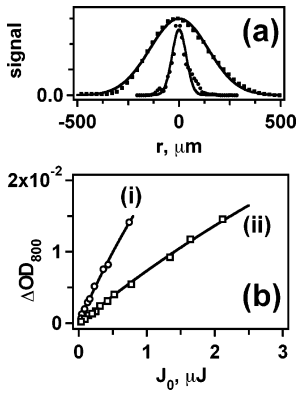

Figure 1. (a) 200 nm pump *(filled circles)* and 800 nm probe *(filled squares)* beam profiles for the photometric experiment in (b). The 1/e radii of these two laser beams were 49 ± 2 and 202 ± 3 μm, respectively. (b) Photoinduced absorbance (800 nm) observed at $t = 5$ ps in 200 nm laser photolysis of aqueous solutions of (i) 0.2 M NaI *(open circles)* and (ii) 0.29 M KOH *(open squares)* vs the total pulse energy J_0 of the 200 nm pump. Solid lines are least-squares fits to eq A3. This 800 nm absorbance signal is from thermalized photoelectrons detached from their parent anions. See sections 2 and 3.1 for more detail.

Ultrafast Quantum Yield Measurements (200 nm Photoexcitation). The pump power, before and after the sample, was monitored using a thermopile power meter (Ophir Optronics model 2A-SH). Normally, the concentration of the anion was such that the optical density of the solution across the jet was 2−3; the transmission of the pump pulse was therefore negligible. For obtaining the power dependence, a fast-response pyroelectric detector was used (Molectron J3−080) whose output was amplified by 20 dB using a three-stage preamp (SRS model 240). This detector was calibrated at 1064 nm, and the readings for 200 nm light were corrected by a factor of 1.43 given by the manufacturer. These readings were 7−10% lower than the readings from the thermopile detector (both of these NIST traceable detectors had been recently calibrated by their respective manufacturers). Two methods were used to characterize radial profiles of the focused beams at the jet surface: (i) transverse scanning of the beams by a 10 μm pinhole and (ii) imaging of the beams using a CCD camera placed in the equivalent focal plane. The typical eccentricity of these focused beams was 1−5%. A harmonic average of 1/e semiaxes obtained by a 2D Gaussian fit is given below as the beam radius (eq A1 in Appendix A; see the Supporting Information). The probe beam was perfectly Gaussian (the typical profiles are shown in Figure 1a), whereas the 200 nm pump beam was of inferior quality, exhibiting one or several "hot" spots. For this reason, absolute quantum yield measurements were performed with the reverse beam geometry: the probe beam enveloped the pump beam and integrated over the imperfections in the latter. For kinetic measurements, the more common geometry was used:

the typical radii of the probe and pump beams were 65 and 210 μm, respectively, so that the pump beam enveloped the probe beam.

Absolute quantum yields for hydroxide and iodide were determined photometrically using an approach explained in Appendix A (see the Supporting Information). A power dependence of the photoinduced 800 nm absorbance from hydrated electron at delay time $t = 5$ ps was plotted vs the total pump energy J_0, and quantum yield ϕ was calculated by least-squares fits using eq A3. For the data shown in Figure 1b, the beam radii of the pump and probe were 49 ± 2 and 202 ± 3 μm, respectively. The absolute quantum yield obtained in this fashion depends on the assumed molar absorptivity of the electron at 800 nm (the value of 18 530 M^{-1} cm^{-1} [21,22] was used throughout this series), the absolute pump power (known to $\pm$5% accuracy due to the uncertainty in the calibration of the power meters), and the radii of the pump and probe beams (known with accuracy <3−5%). The thickness of the jet and the absorbance of photoexcitation light by the solution need not be known precisely for the quantum yield determination.

These photometric measurements were complemented by actinometry. Electron generation in 200 nm photoexcitation of $K_4Fe(CN)_6$ was the primary actinometric standard; $\phi_0 = 1$ was assumed for this photoreaction (section 3.2). A 1.4 μm thick film of amorphous hydrogenated silicon on a Suprasil substrate (obtained from H. Fritzsche of the University of Chicago) was used as the secondary standard. This sample was mounted on a 2D translation stage and positioned into the plane of the jet; the pump and probe beams passed through the same spot of this sample for each measurement. For each anion solution, this reference sample was inserted into the beam path immediately after the kinetic measurement. The 800 nm absorbance taken at the end of the excitation pulse was used for the normalization of e_{aq}^- kinetics from these anion solutions. This 800 nm absorbance signal (ca. 0.134 OD per 1 μJ of incident pulse energy for a 59 μm 1/e radius pump beam, see Figure 1S in the Suporting Information) was linear to the highest pump fluence used for anion photoexcitation. The last step was to normalize these scaled electron kinetics so that the prompt electron yield for $Fe(CN)_6^{4-}$ was unity. For the series shown in Figure 2, the pump power was 0.1−0.3 μJ, and Gaussian radii for the pump and probe beams were 43−46 and 13−20 μm, respectively.

225 and 242 nm Photoexcitation. Kinetic experiments with 225 nm (242 nm) photoexcitation were carried out at USC using either a 200 or a 1 kHz Ti:sapphire amplified laser system for which details are given elsewhere.[4,5,6] A 1 mm optical path cell with CaF_2 windows was used to flow the sample. Transient absorption signals down to 10 μOD can be studied using this pump−probe spectrometer. Photoexcitation pulses were generated by frequency doubling or mixing the pumped OPA output. The probe pulses (500 or 700 nm) were selected from the white light supercontinuum generated in a sapphire disk using a 25 nm fwhm band-pass interference filter. In dilute hydrosulfide solutions (<0.01 M), 2-photon water ionization by 242 nm light competed with 1-photon electron detachment from HS^- when the 242 nm light irradiance was >20 GW/cm^2. To avoid this complication, 0.04−0.14 M HS^- solutions were used and the laser irradiance was kept <5 GW/cm^2. Under these conditions, two photon ionization of water was negligible, and the transient kinetics did not change with the HS^- concentration and pump irradiance.

3. Results

3.1. Photometric Quantum Yield Measurements for 200 nm Photolysis of Hydroxide and Iodide. Power dependencies for the yield of hydrated electron were obtained at delay time $t = 5$ ps following a 200 nm (300 fs fwhm) photoexcitation of 0.29 M KOH and 0.2 M NaI solutions (Figure 1b). At this delay time, the thermalization/solvation of the electron is complete. No species other than the electron absorbed at the probe wavelength of 800 nm. The time profile of the thermalization and geminate decay kinetics did not change with the 200 nm pump power (to 2.5 μJ). The negative curvature in these power dependencies is the consequence of the beam geometry, as explained in the Appendix A.

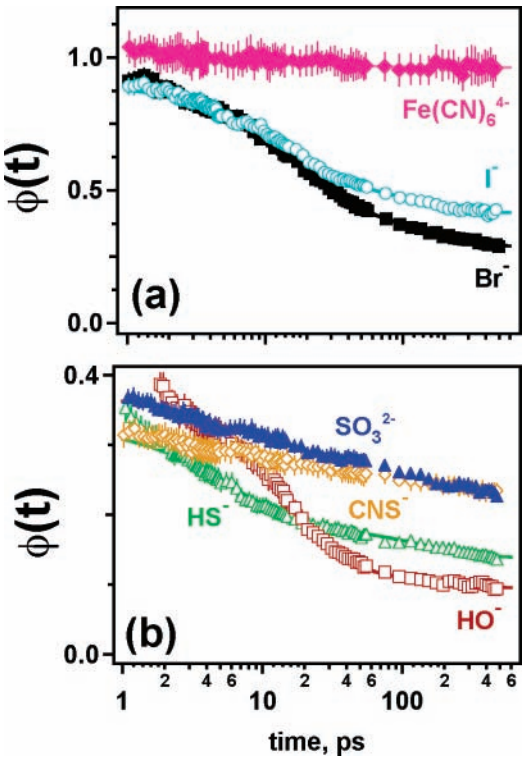

Figure 2. Time-dependent quantum yield $\phi(t)$ of photoelectrons vs delay time t of 800 nm probe pulse. See section 3.2 for more detail. Single 200 nm photon excitation of aqueous (a) iodide *(open circles, cyan)*, bromide *(filled squares, black)*, and ferrocyanide *(filled diamonds, pink)* and (b) hydroxide *(open squares, red)*, hydrosulfide *(open triangles, green)*, thiocyanate *(open diamonds, yellow)*, sulfite *(filled triangles, blue)*. The anion concentrations are given in the first column of Table 1.

Quantum yields $\phi_0 \approx 0.95$ for iodide and $\phi_0 \approx 0.34$ for hydroxide were obtained by fitting these power dependencies using eq A3. The confidence limits are $\pm$10% due to the uncertainty in the assumed parameters (section 2). Near unity ϕ_0 for electron detachment in 225−255 nm photolysis of aqueous iodide was (indirectly) determined by Bradforth and co-workers,[4] who extrapolated the free electron yield data of Iwata et al. (for 248 nm photolysis) to $t \rightarrow 0$ using their ultrafast kinetic data.

3.2. Actinometric Quantum Yield Measurements for Various Anions (200 nm Photoexcitation). The concentrations of the anions studied and their molar absorptivities at 200 nm are given in Table 1 (the latter were taken from the literature sources given in Table 2 of part 1 of this series).[1] Time dependencies of quantum yield $\phi(t)$ for the electron in 200 nm photoexcitation of these aqueous anions were obtained as described in section 2 and then fit between 3 and 600 ps by a sum of two exponentials with a nonzero offset (Figure 2). The prompt and terminal quantum yields given in Table 1, ϕ_0 and ϕ_∞, respectively, were extrapolated to $t \rightarrow \infty$ and $t \rightarrow 0$ using these biexponential fits, and the ratio ϕ_∞/ϕ_0 of these quantities

TABLE 1: Actinometric Estimates for Quantum Yields ϕ of Hydrated Electron in 200 nm Photolysis of Aqueous Anions at 23 °C[a]

anion	a	ϵ_{200}[b]	$\phi_{t\to 0}$	ϕ_{10ps}	ϕ_∞	Ω_∞,[c] ×100	ϕ_∞[d] 248 nm	ϕ_∞[d] 193 nm
I^-	20	10	0.901	0.715	0.415	46.1	0.286	0.497
Br^-	20	10	0.906	0.697	0.292	31.8		0.365
HO^-	200	1	0.378	0.261	0.092	24.5		0.112
HS^-	40	5.6	0.329	0.214	0.139	42.2	0.014	0.298
CNS^-	25	0.8−1	0.304	0.282	0.231	76.2	0.019	0.306
SO_3^{2-}	40	6.3	0.353	0.313	0.231	65.4	0.108	0.391
$[KFe(CN)_6]^{3-}$	20	13.07	1.0	0.995	0.963	>96	0.674	1.018

[a] millimolar concentration of the anion in the photolyzate. [b] Molar absorptivity of the anion at 200 nm, in 10^3 M^{-1} cm^{-1}. [c] Survival probability of the geminate electron/radical pair. [d] Terminal quantum yields ϕ_∞ for free electron formation in 248 and 193 nm photolysis (from ref 1). [e] ϕ_{10ps}, $\phi_{t\to 0}$, and ϕ_∞ are the quantum yield determined experimentally at $t = 10$ ps and the prompt and terminal quantum yields extrapolated to $t = 0$ and $t = \infty$, respectively, as described in the text.

TABLE 2: Simulation Parameters for Geminate Pairs Derived from Monovalent Anions

anion	λ*, nm[a]	p_d	α[b]	W^{-1}, ps	υ
I^-	225	0.216	0.34	14.0	*c*
	200				2.17
Br^-	200, 225	0.268	0.57	16.5	*c*
HO^-	200	0.173	0.375	12.0	*c*
	242				*c*
HS^-	225	0.121	0.306	3.5	3.03
	200				2.14

[a] Photoexcitation wavelength. [b] Dimensionless parameter $\alpha = p_d\sqrt{a^2W/D}$. [c] $\upsilon \gg 1$.

provided an estimate for the survival probability Ω_∞ of the corresponding geminate pair (Table 1). For convenience, quantum yields at $t = 10$ ps are also given. Note that the ratio of ϕ_0 for hydroxide and iodide determined actinometrically is 0.36, which equals the ratio of photometric ϕ_0 given in section 3.1. For comparison, free electron yields for 248 and 193 nm laser photoexcitation of the same anions are also given in Table 1.

Figure 2 suggests that aqueous hexacyanoferrate(II) anion (commonly referred to as ferrocyanide) has the highest ϕ_0 the aqueous anions studied in this work. The geminate decay for ferrocyanide is very slow; there is almost no decay of the electron absorbance over the first 600 ps. Bradforth and co-workers observed <20% decrease in the hydrated electron absorbance over the first 1.5 ns after 225 nm photoexcitation of ferrocyanide and no detectable variation in the survival probability over 400 ps for excitation wavelengths covering 225−300 nm.[23] For higher photon energy, this geminate decay may be even slower, since Sauer et al. obtained $\phi_\infty \approx 1$ for electron formation in 193 nm photolysis of 0.05−0.7 mM ferrocyanide.[1] A limiting quantum yield ϕ_∞ of 0.88 for 214 nm photolysis was determined by Shirom and Stein.[24] Between 254 and 214 nm wavelength, ϕ_∞ rapidly increased with the photon energy.[24] For all of these reasons, ϕ_0 for ferrocyanide was taken as unity. We emphasize that in millimolar solution, ferrocyanide is associated with one or two potassium cations.[23,25] The first association constant is ca. 180 M^{-1},[25] i.e., 55% and 92% of the anions are associated in 2 and 20 mM solutions, respectively. The associated anions may have slightly different photochemical properties than bare anions (see parts 1[1] and 2[11] of this series). Nevertheless, no difference was observed in the recombination dynamics for 2 and 20 mM ferrocyanide solutions (see Figure 4b in section 4.1). Another complication is the occurrence of protic equilibria[26,27] and hemicolligation[28,29] that is discussed in Appendix B in the Supporting Information. It is shown there that (with the exception of the carbonate anion) these side reactions do not present concern in the concentration and time regimes studied.

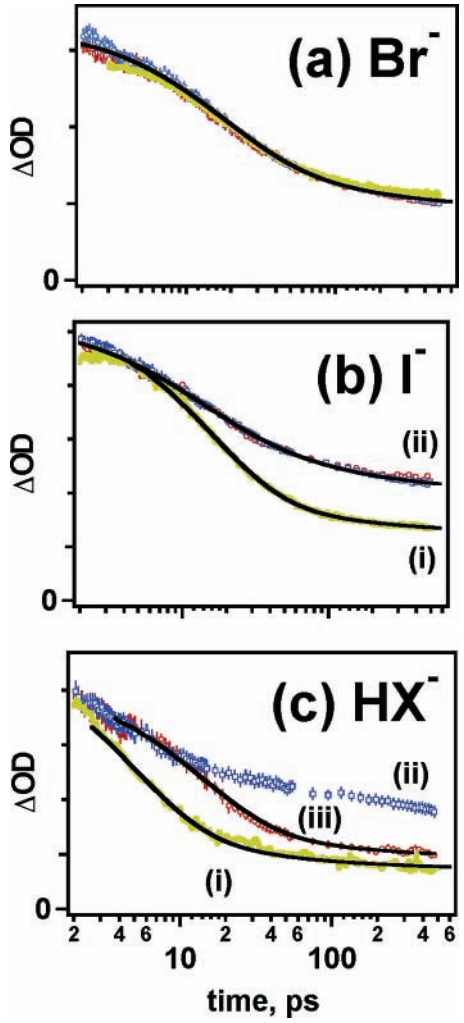

Figure 3. Normalized transient absorbance signals from thermalized photoelectrons generated in laser photolysis of aqueous (a) bromide, (b) iodide, and (c) hydrosulfide *(i,ii)* and hydroxide *(iii)*. In each panel, the symbols indicate the kinetics obtained by 200 nm photoexcitation of these anions, and the decays are seen to be invariant to the probe wavelength (800 nm, red squares; 1000 nm, blue circles). The yellow lines in each panel are data taken with longer wavelength photoexcitation for each anion. For bromide and iodide, photoexcitation is at 225 nm (a and b, trace i); for hydrosulfide, photoexcitation is 242 nm (c, trace i). For each yellow line, the probe wavelength is 700 nm.

3.3. Geminate Recombination: A Comparison between the High and Low Energy Excitation Data. In this section, 200 nm pump−800 nm probe kinetics are compared with these kinetics obtained for 225 or 242 nm photoexcitation (Figures 3

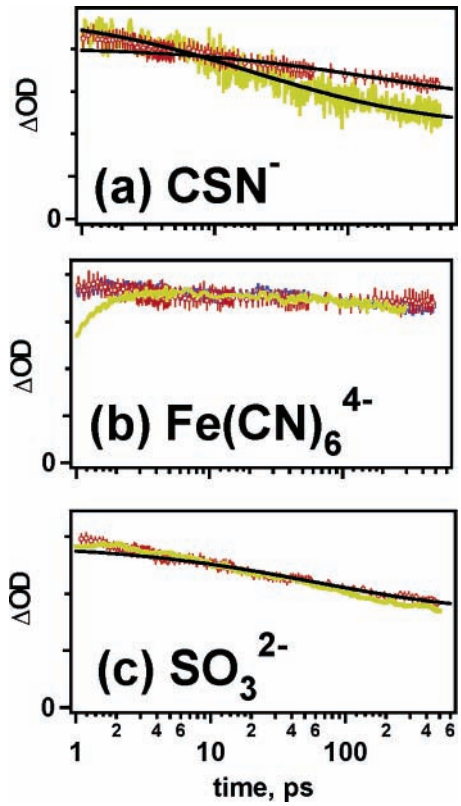

Figure 4. Same as Figure 3, for (a) thiocyanate, (b) ferrocyanide, and (c) sulfite. The symbols are for 200 nm photoexcitation, the *(yellow)* lines are for 225 nm (a, b) and 242 nm (c) photoexcitation. *(Black)* solid lines are least-squares fits obtained using the free diffusion model given in section 4.1 assuming the r^2-exponential distribution of photoelectrons. In part b, kinetics obtained by 200 nm photoexcitation of 2 mM *(open squares, blue)* and 20 mM *(open circles, red)* ferrocyanide are given in the same plot, for comparison.

and 4). In the latter series the probe wavelength was 700 nm unless specified otherwise. Because of the differences in the probe wavelength and the width of the pump pulse, only kinetics at $t > 5$ ps were compared (in the figures given below, these two sets of kinetics were normalized at 5−10 ps; e.g., Figure 3a).

Figure 3a demonstrates these two normalized kinetics for bromide. This anion has the first absorption maximum of CTTS band at 200 nm.[27,30,31] The 200 and 225 nm kinetics are exactly the same. For (I,e_{aq}^-) pair, the time profile of recombination kinetics does not depend on the photon energy when it is scanned across the low energy (225 nm) CTTS subband of this anion.[4,6] Apparently, the decay kinetics for the (Br,e_{aq}^-) pair follow the same pattern. In ref 6, recombination dynamics of (I,e_{aq}^-) pairs for *higher* excitation energies were studied systematically as a function of the total photon energy using *biphotonic* excitation of iodide. For this anion, the kinetics observed after one- and two-photon excitation of the same total energy are nearly the same[6] (which is not the case for OH^-).[10] Given these previous results, only two iodide traces are given in this study as a reference, to contrast the 200 and 225 nm kinetics for the iodide (Figure 3b) with such kinetics for bromide (Figure 3a). The 200 nm photoexcitation corresponds to the second (192 nm) CTTS subband of the iodide.[6,27,30] The 200 and 225 nm kinetics for I^- are very different: for the 200 nm photoexcitation, the survival probability is greater and the fast exponential component is less prominent. As argued in ref 6, this transformation is consistent with broadening of the initial spatial distribution of photogenerated electrons in the course of 200 nm photoexcitation.

Figure 3c, traces i and ii, shows 242 and 200 nm kinetics for HS^-, respectively. For this anion, the maximum of the first CTTS band in water is at 228 nm;[32] 200 nm is close to the position of its second CTTS band ("D" band).[32] Thus, energetically the situation is very similar to I^-. The transformation of the decay kinetics observed at the higher photoexcitation energy strikingly resembles that observed for I^- in Figure 3b. Except for the faster exponential component (that fully decays in 20 ps), the 242 nm kinetics for HS^- look similar to those observed in 200 nm photoexcitation of HO^- (Figure 3c, trace iii) and Br^- (and 255−225 nm photoexcitation of iodide), whereas the 200 nm kinetics for HS^- look more like those for 200 nm photoexcitation of I^- (compare Figure 3b, trace ii, and Figure 3c, trace ii).

For anions other than halide and HO^-/HS^-, few generalizations can be made except for the lack of the fast component. Even for CSN^-, which is a pseudohalide anion, the 225 and 200 nm kinetics look qualitatively different from other (pseudo-)halide anions (compare Figures 3 and 4a). No fast component is discernible for either photoexcitation energy; the decay of the electron is very slow and the survival probability Ω_∞ of the geminate pair is high. The latter value is ca. 20% greater for 200 nm photoexcitation than for 225 nm photoexcitation. These kinetics look similar to those obtained for polyvalent anions, such as sulfite (Figure 4c); the only difference is the relatively low ϕ_0 for CSN^-. For polyvalent anions, there is a general trend on gradual increase in Ω_∞ with the excitation energy. This is illustrated by the 200 and 242 nm kinetics for sulfite (Figure 4c), (the survival probability at 600 ns is ca. 10% higher for the higher photon energy). This increase does not occur for ferrocyanide (Figure 4b), since $\phi_\infty \approx 1$ even at low excitation energy;[23] the apparent differences between the 200 and 225 nm kinetics (observed for $t < 3$ ps) originate through the difference in the probe wavelength used to observe the electron dynamics (800 and 500 nm, respectively).

For all of the anions studied, both mono- and polyvalent, the survival probability Ω_∞ either increases with the photoexcitation energy or, at least, stays the same. A systematic increase in Ω_∞ with increasing photoexcitation energy has been observed by Schwartz and co-workers for Na^- in THF.[8] Bradforth and co-workers observed an increase in the survival probability with the *total* excitation energy of biphotonic photoexcitation of I^-.[6] Apparently, this trend pertains to all CTTS anions regardless of the solvent and/or photoexcitation mode.

4. Discussion

4.1. Simulation of Kinetic Traces for Polyvalent Anions. For polyvalent anions and CNS^-, a free diffusion model complemented with a prescribed initial distribution $P(r_i)$ of the electrons around their parent radicals provides a starting point for simulating geminate pair dynamics. Hereafter, we assume spherically symmetrical distribution $P(r_i)$ of the electrons and the mean force potential $U(r)$ for the geminate partners. In the free diffusion model,[13] the interaction between these geminate partners is neglected (i.e., $U(r) = 0$), and the pair decays via diffusion-controlled recombination at the contact radius $r = d$. The survival probability $\Omega(t)$ for a pair generated at a distance $r = r_i$ is given by

$$\Omega(t) = 1 - (d/r_i)\,\mathrm{erfc}[(r_i - d)/2\sqrt{Dt}] \qquad (1)$$

where D is the mutual diffusion coefficient. The survival probability of the geminate pairs is given by $\Omega_\infty = 1 - \langle d/r_i \rangle$, which is a function of the initial distribution $P(r_i)$ of the electron

only. Equation 1 is averaged over this initial distribution. The empirical distribution $P(r_i)$ that gave the best results was an r^2-exponential distribution with average width $\langle r_i \rangle = 3b_E$,

$$4\pi r_i^2 P(r_i) = (2b_E^3)^{-1} r_i^2 \exp(-r_i/b_E) \quad (2)$$

(an r^2-Gaussian distribution provided equally good fits to these data). In these simulations, we assumed that $d = 0.5$ nm and $D = 4.5 \times 10^{-5}$ cm^2/s (which is the diffusion coefficient for hydrated electron in pure water). Only $t > 5$ ps kinetics were used to obtain the least-squares fit. A typical fit for 200 nm photoexcitation of sulfite is shown in Figure 4c. The following optimum parameters were obtained: $b_E = 0.39 \pm 0.01$ nm ($\langle r_i \rangle = 1.3$ nm) and $\Omega_\infty = 0.53$. For 242 nm photoexcitation, $b_E = 0.32 \pm 0.04$ nm ($\langle r_i \rangle = 1.1$ nm) and $\Omega_\infty = 0.47$; i.e., the escape probability is ca. 13% higher for the 200 nm photoexcitation. Note that this increase is clearly insufficient to account for a two times increase in the free electron yield between 248 and 200 nm (Table 1) for sulfite. Apparently, for this anion the *prompt* quantum yield of the electron *increases* with the photon energy.

For thiocyanate anion excited by 200 and 225 nm photons, we obtained $b_E = 0.61 \pm 0.08$ nm ($\langle r_i \rangle = 1.92$ nm) and $\Omega_\infty = 0.66$ and $b_E = 0.26 \pm 0.09$ nm ($\langle r_i \rangle = 0.98$ nm) and $\Omega_\infty = 0.41$, respectively (for the r^2-exponential distribution). Thus, the escape probability increases by 60% from 242 to 200 nm photoexcitation, whereas the free electron yield increases more than 10 times from 248 to 200 nm (Table 1). Once more, the dramatic increase in ϕ_∞ can only be due the increase in the *prompt* electron yield rather than the survival probability of the geminate pair.

For ferrocyanide, geminate recombination is so slow and inefficient that only a lower estimate for $\langle r_i \rangle$ can be obtained, ca. 3.1 nm (which would correspond to $\Omega_\infty = 0.66$; compare this estimate with ca. 2 nm obtained in ref 23 using a model including Coulomb repulsion). For all of the anions, the average ejection distances $\langle r_i \rangle$ are over 1 nm, which is the typical electron−hole separation in the low-energy excitation of neat water (section 1). This suggests that the electron promoted from photoexcited polyvalent anions may be ejected directly into the conduction band of the solvent.

Hydrosulfide is a monovalent anion for which the geminate dynamics observed following 200 nm photoexcitation may, on principle, be simulated using eq 1 and an ad hoc electron distribution $P(r_i)$ shown in Figure 2S in the Supporting Information (note that for monovalent anions other than thiocyanate, no distribution $P(r_i)$ can be found to account for the kinetics observed, provided that the diffusion is free). This distribution was determined by the least-squares optimization of probability weights. The optimum distribution consists of a narrow peak at $r_i < 1$ nm (that includes 84% of the electrons with $\langle r_i \rangle$ of 0.63 nm) and a broad peak centered at 2.4 nm (which includes 16% of the electrons with $\langle r_i \rangle$ of 3 nm). These simulation parameters suggest that the diffuse component of the electron distribution for HS^- photoexcited by 200 nm light might be at least as broad as that for CSN^-. Note that for HS^- excited by 242 and 200 nm photons, the escape probability of the electron (as estimated from biexponential fits) changes with the photon energy ca. 3 times, whereas the free electron yield changes by an order of magnitude from 248 to 200 nm (Table 1). This anion provides yet another example of an anion photosystem in which ϕ_0 dramatically increases with the photoexcitation energy.

4.2. Simulation of Kinetic Traces for Monovalent Anions. The approach used to simulate kinetics for geminate pairs derived from monovalent anions is based on Shushin's semi-analytical theory[6,10,11,33] for diffusion-controlled reactions in a potential well. In this model, geminate partners interact by means of an *attractive* mean force potential (MFP), $U(r)$, with Onsager radius a (at which $U(a) \approx -kT$). It can be shown that the recombination and escape from the potential well are pseudo-first-order reactions; the corresponding constants W_r and W_d can be evaluated in a rather complex way from the radial profile of the MFP and the diffusion constant D.[10,33] The survival probability $\Omega(t)$ is given by[10]

$$\Omega(t) \approx 1 - (1 - p_d)\left[1 + \frac{\mathbf{Im}\, \lambda^{-1} \exp(\lambda^2 Wt)\, \mathrm{erfc}(\lambda\sqrt{Wt})}{\mathbf{Im}\, \lambda}\right] \quad (3)$$

where $W = W_r + W_d$ is the total decay rate, $p_d = W_d/W$ is the escape probability of a geminate pair generated in the potential well ($r_i < a$), and $\lambda = \alpha/2 + i(1 - \alpha^2/4)^{1/2}$, where $\alpha = p_d\sqrt{a^2 W/D}$ is a dimensionless parameter. On a short time scale ($Wt \ll 1$), the survival probability $\Omega(t)$ decays exponentially as $\exp(-Wt)$, whereas on a long time scale ($Wt \gg 1$), it decays by a power law as $p_d(1 + a/\sqrt{\pi t D})$, asymptotically approaching p_d at $t \rightarrow \infty$. In the derivation of eq 3, it was assumed that all of the geminate pairs were generated inside the potential well (that is, $r_i < a$). In a more general case, Sushin's equations must be averaged over the initial electron distribution $P(r_i)$ of the electrons; a compact analytical expression similar to eq 3 cannot be obtained in such a case but a numerical solution can be computed from the Laplace transform of $\Omega(t)$ using eqs B11 and B24 given in Appendix B of ref 10. The escape probability Ω_∞ for an arbitrary electron distribution is given by

$$\Omega_\infty = 1 - (1 - p_d)\langle \min(1, a/r_i) \rangle \quad (4)$$

(see eq B25 in ref 10). For an r^2-exponential distribution, eq 4 simplifies to

$$\Omega_\infty = p_d + (1 - p_d)\exp(-\upsilon)[1 + \upsilon/2] \quad (5)$$

(see eq B28 in ref 10), where another dimensionless parameter, $\upsilon = 3a/\langle r_i \rangle$ is introduced. For $\upsilon \gg 1$, $\Omega_\infty = p_d$ and $\Omega(t)$ is given by eq 3. Note that in Shushin's theory all geminate pairs for which $r_i < a$ have the same recombination dynamics, so that the overall kinetics are not sensitive to the exact profile of $P(r_i)$ at these short distances.

For halide anions, I^- and Br^-, the kinetics do not change with the photoexcitation energy across the low energy CTTS subband, and we assume that the electron distribution does not change with this energy. (It may also be assumed that in this energy regime $\upsilon \gg 1$, and the geminate kinetics are not sensitive to the changes in the electron distribution for $r_i < a$.) The optimum fit parameters (α, p_d, W^{-1}) are given in Table 2. The model parameters are similar for both of these halide anions, with a greater escape probability p_d, residence time W^{-1} and estimated Onsager radius a for bromide (0.58 vs 0.42 nm; these Onsager radii were estimated assuming a value of 4.5×10^{-5} cm^2/s for the diffusion coefficient D). These parameters are close to those obtained for hydroxide (Table 2); the Onsager radius a for the (OH,e_{aq}^-) pairs is ca. 0.53 nm. As shown in ref 6, for iodide excited by photons with total energy > 6 eV, the kinetics can still be fit using the same MFP parameters assuming that the electron distribution exhibits a broad, diffuse component in addition to the narrow ($\upsilon \gg 1$) distribution typical of the low-energy CTTS photoexcitation. The broad and the narrow components can be interpreted as the direct ionization and CTTS

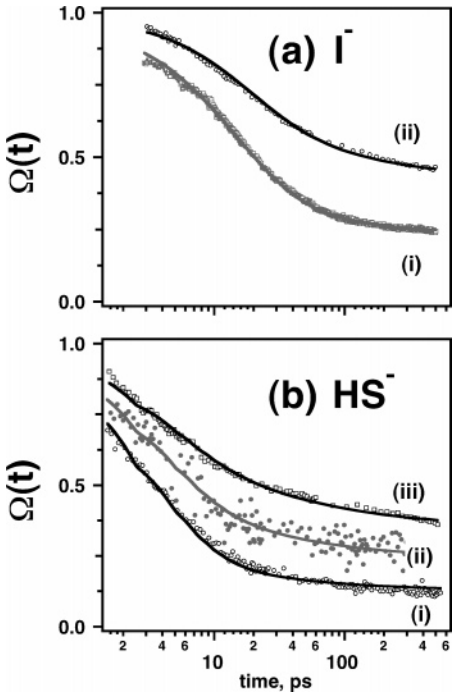

Figure 5. Time-dependent survival probability $\Omega(t)$ of the geminate pairs vs reduced time Wt (section 4.2). The simulation parameters obtained from least-squares fits to the generalized Shushin's model equations are given in Table 2. The geminate (X,e_{aq}^-) pairs are generated by (a) 225 nm *(i)* and 200 nm *(ii)* photoexcitation of aqueous iodide and (b) 242 nm *(i)*, 225 nm *(ii)*, and 200 nm *(iii)* photoexcitation of aqueous hydrosulfide.

state mediated electron detachment, respectively. A monomodal (e.g., r^2-exponential) distribution with b_E increasing smoothly with the photon energy provided a rather poor overall fit for the kinetics;[6] the best quality multitrace fit was obtained by letting the weights of the narrow ($r_i < a$) and broad ($r_i > a$) distribution be floating parameters as a function of the excitation energy. To fit the 200 nm data for the iodide, such a bimodal distribution is not needed: it is possible to fit the kinetic data using the r^2-exponential distribution (Table 2). The choice between the bimodal and monomodal distribution is difficult to make since the shape of this prescribed monomodal distribution is arbitrary. The advantage of using the bimodal distribution is that the two postulated components have clear physical meaning. The disadvantage is that extra assumptions have to be made to reduce the parameter space (e.g., in ref 6, we assumed that the broad distribution has the same width at different energies, which is not self-evident, etc.) Such a dilemma is always present in the analysis of recombination kinetics due to the relatively weak dependence of $\Omega(t)$ on the fine details of the $P(r_i)$ profile.

The broad initial electron distribution is also needed to account for the HS^- kinetic traces ii and iii given in Figure 5b. Following the approach used for iodide[4,6] and hydroxide,[10] we assumed that the lowest-energy (242 nm) kinetics correspond to the case when $\upsilon \gg 1$ and then optimized parameter υ; this procedure gave $\upsilon \approx 3$ for 225 nm photoexcitation and $\upsilon \approx 2.1$ for 200 nm photoexcitation. Note that for hydrosulfide the lifetime of caged pairs (parameter W^{-1}) is 3−5 times shorter than that for OH^- and halide anions (Table 2); the Onsager radius is also smaller (ca. 0.32 nm). The probability of escape, p_d, at the onset of the CTTS band, increases in the order $Br^- > I^- > OH^- > HS^-$.

5. Concluding Remarks

Time-dependent photoelectron quantum yields generated by 200 nm photoexcitation of several aqueous anions have been obtained. These kinetic profiles were compared with the 225 nm (and/or 242 nm) kinetic data for the same anions. It is shown that electron photodetachment from molecular anions is qualitatively different from the electron photodetachment from halide anions. In particular, the distribution of electrons promoted from nonhalide anions (including HS^-, CSN^- and all polyvalent anions) shows a broad component from the very onset of the lower CTTS band. Photoexcitation of polyvalent anions as well as some pseudohalide anions, such as CSN^-, *always* yields this broad distribution, regardless of the photon energy. For halide anions, the electron distribution changes from a narrow one to a broad one when the photon energy exceeds a certain threshold value.[4,6] There is a systematic broadening of the electron distribution with the excitation energy (e.g., for SO_3^{2-}, CSN^-, and I^-) that accounts for the increase in the survival probability Ω_∞ and contributes to the larger free electron yield $\phi_\infty = \phi_0\Omega_\infty$.

For aqueous halides, $\phi_0 \approx 1$ regardless of the photoexcitation energy, but this is not the case for other anions. Even pseudohalide anions such as HO^- and HS^- (for which there are no known side photoreactions or discernible bound-to-bound absorbances)[1] exhibit ϕ_0 substantially lower than unity (Table 1). For ferrocyanide, CSN^-, SO_3^{2-}, and HS^-, ϕ_0 is small at low energy and the yield progressively *increases* with the increasing photoexcitation energy. For 200 nm photoexcitation, ϕ_0 for pseudohalides are 30−40% of the quantum yields for halides; the ϕ_0 for polyvalent anions do not follow any obvious pattern.

Theoretical studies of Sheu and Rossky[14] on halide CTTS suggest that the broad electron distribution might originate through the direct injection of the electron into the conduction band of water from the CTTS state. For some anions (e.g., ferrocyanide),[34] the ejection distances are so long that no other mechanism seems possible. The broadening of the electron distribution with increasing excitation energy may be viewed as a competition between this direct ionization (which involves extended state electrons) and dissociation of the precursor CTTS state that involves localized electrons only.[6] The latter photoprocess would prevail at low excitation energies since the conduction band is inaccessible at these low energies.

Our results do not wholly agree with this "competition" picture: for some anions (both mono- and polyvalent) the broadening of the electron distribution with increasing excitation energy occurs across their entire lower CTTS band. For polyvalent anions (and even some monovalent anions, such as thiocyanate), it is not apparent from our kinetic data that the CTTS state dissociation (with the formation of a caged pair) analogous to the one observed for I^-, Br^-, HO^-, and HS^- occurs at all, possibly due to the Coulomb repulsion between the emerging localized electron and the residual radical anion.

Energetics alone do not account for the remarkable differences observed between the picosecond dynamics of the corresponding geminate pairs. For example, HS^-, I^-, CSN^-, and SO_3^{2-} all have similar CTTS band energies and photoelectron emission threshold energies (see Table 1 in ref 34), yet CSN^- and SO_3^{2-} yield broad electron distributions regardless of the photoexcitation energy whereas I^- and HS^- yield a narrow electron distribution when excited by low energy photons and a broad electron distribution when excited by high energy photons. Such results hint at the multiplicity of reaction pathways for the charge separation process.[23]

From the outset of photochemical studies of CTTS anions, it has been believed that studies of electron photodetachment from halides, such as iodide, would provide critical insight into the analogous photoreactions for more complex polyatomic anions. This work suggests that even the simplest polyatomic anions behave somewhat differently from these halides. More experimental and theoretical studies are therefore needed before any generalization is possible. In particular, theoretical modeling of CTTS state dissociation for polyatomic, especially polyvalent, anions would be beneficial since presently such models exist for halide anions only. The latter appear to be in a class of their own.

Acknowledgment. We thank M. C. Sauer, Jr., C. D. Jonah, D. M. Bartels, S. Pimblott, B. J. Schwartz, and S. V. Lymar for many useful discussions. The research at the ANL was supported by the Office of Science, Division of Chemical Sciences, US-DOE under Contract No. W-31-109-ENG-38. Victor Vilchiz and Victor Lenchenkov (USC) are thanked for experimental data included in this paper. The research at USC was supported by the National Science Foundation (Grant No. CHE 0311814) and the David and Lucile Packard Foundation. S.E.B. is a Cotrell Scholar of the Research Corporation.

Supporting Information Available: A PDF file containing Appendix A, equations for the absolute quantum yield measurement, and Appendix B, protic equilibria and secondary chemistry, and Figures 1S−3S (transient absorbance, time dependent quantum yield, and fitting of excitation kinetics, respectively) with captions. This material is available free of charge via the Internet at http://pubs.acs.org.

References and Notes

(1) Sauer, M. C., Jr.; Crowell, R. A.; Shkrob, I. A. *J. Phys. Chem. A* **2004**, *108*, 5490.

(2) Blandamer, M. J.; Fox, M. F. *Chem. Rev.* **1970**, *70*, 59.

(3) Bradforth, S. E.; Jungwirth, P. *J. Phys. Chem. A* **2002**, *106*, 1286.

(4) Kloepfer, J. A.; Vilchiz, V. H.; Lenchenkov, V. A.; Chen, X.; Bradforth, S. E. *J. Chem. Phys.* **2002**, *117*, 776.

(5) Vilchiz, V. H.; Kloepfer, J. A.; Germaine, A. C.; Lenchenkov, V. A.; Bradforth, S. E. *J. Phys. Chem. A* **2001**, *105*, 1711. Kloepfer, J. A.; Vilchiz, V. H.; Germaine, A. C.; Lenchenkov, V. A.; Bradforth, S. E. *J. Chem. Phys.* **2000**, *113*, 6288. Kloepfer, J. A.; Vilchiz, V. H.; Lenchenkov, V. A.; Bradforth, S. E. In *Liquid Dynamics: Experiment, Simulation, and Theory* 2002, Vol. 820, pp 108. Kloepfer, J. A.; Vilchiz, V. H.; Lenchenkov, V. A.; Bradforth, S. E. *Chem. Phys. Lett.* **1998**, *298*, 120.

(6) Chen, X.; Kloepfer, J. A.; Bradforth, S. E.; Lian, R.; Crowell, R. A.; Shkrob, I. A., manuscript in preparation.

(7) Barthel, E. R.; Martini, I. B.; Keszei, E.; Schwartz, B. J. *J. Chem. Phys.* **2003**, *118*, 5916. Martini, I. B.; Barthel, E. R.; Schwartz, B. J. *J. Am. Chem. Soc.* **2002**, *124*, 7622. Barthel, E. R.; Martini, I. B.; Schwartz, B. J. *J. Chem. Phys.* **2000**, *112*, 9433.

(8) Barthel, E. R.; Schwartz, B. J. *Chem. Phys. Lett.* **2003**, *375*, 435.

(9) Gauduel, Y.; Hallou, A.; Charles, B. *J. Phys. Chem. A* **2003**, *107*, 2011. Gauduel, Y.; Hallou, A. *Res. Chem. Intermed.* **2001**, *27*, 359. Gauduel, Y.; Gelabert, H.; Ashokkumar, M. *Chem. Phys.* **1995**, *197*, 167. Gelabert, H.; Gauduel, Y. *J. Chem. Phys.* **1996**, *100*, 3993. Long, F. H.; Shi, X.; Lu, H.; Eisenthal, K. B. *J. Phys. Chem.* **1994**, *98*, 7252; *Chem. Phys. Lett.* **1990**, *169*, 165.

(10) Lian, R.; Crowell, R. A.; Shkrob, I. A.; Bartels, D. M.; Chen, X.; Bradforth, S. E. *J. Chem. Phys.* **2004**, *120*, 11712.

(11) Sauer, M. C., Jr.; Lian, R.; Crowell, R. A.; Bartels, D. M.; Shkrob, I. A.; Chen, X.; Suffern, D.; Bradforth, S. E. *J. Phys. Chem. A* **2004**, *108*, 10414.

(12) Iwata, A.; Nakashima, N.; Kusaba, M.; Izawa, Y.; Yamanaka, C. *Chem. Phys. Lett.* **1993**, *207*, 137.

(13) Rice, S. A. *Diffusion-limited reactions*; Bamford, C. H., Tipper, C. F. H., Compton, G., Eds.; Elsevier: Amsterdam, 1985.

(14) Sheu, W.-S.; Rossky, P. *J. Chem. Phys. Lett.* **1993**, *202*, 186 and 233; *J. Am. Chem. Soc.* **1993**, *115*, 7729; *J. Phys. Chem.* **1996**, *100*, 1295.

(15) (a) Borgis, D.; Staib, A. *J. Chem. Phys.* **1996**, *104*, 4776 and 9027. (b) Borgis, D.; Staib, A. *Chem. Phys. Lett.* **1994**, *230*, 405; *J. Chim. Phys.* **1996**, *93*, 1628*; J. Phys.: Condens. Matter* **1996**, *8*, 9389; *J. Mol. Struct.* **1997**, *436*, 537; *J. Chem. Phys.* **1995**, *103*, 2642.

(16) Smallwood, C. J.; Bosma, W. B.; Larsen, R. E.; Schwartz, B. J. *J. Chem. Phys.* **2003**, *119*, 11263.

(17) e.g., Choi, H. T.; Sethi, D. S.; Braun, C. L. *J. Chem. Phys.* **1974**, *78*, 2128 and references therein.

(18) E.g., Bernas, A.; Ferradini, C.; Jay-Gerin, J.-P. *Chem. Phys.* **1997**, *222*, 151. Bernas, A.; Grand, D. *J. Phys. Chem.* **1994**, *98*, 3440. Sander, M. U.; Luther, K.; Troe, J. *Ber. Bunsen-Ges. Phys. Chem.* **1993**, *97*, 953.

(19) Crowell, R. A.; Bartels, D. M. *J. Phys. Chem.* **1996**, *100*, 17940.

(20) Bartczak, W. M.; Pernal, K. *Res. Chem. Intermed.* **2001**, *27*, 891. Hilczer, M.; Bartczak, W. M. *Radiat. Phys. Chem.* **1992**, *39*, 85. Bartczak, W. M.; Sopek, M.; Kroh, J. *Radiat. Phys. Chem.* **1989**, *34*, 93 and references therein. Goulet, T.; Bernas, A.; Ferradini, C.; Jay-Gerin, J.-P. *Chem. Phys. Lett.* **1990**, *170*, 492. Houee-Levin, C.; Tannous, C.; Jay-Gerin, J.-P. **1989**, *93*, 7074.

(21) Elliot, A. J.; Ouellette, D. C.; Stuart, C. R. *The Temperature Dependence of the Rate Constants and Yields for the Simulation of the Radiolysis of Heavy Water*; AECL report 11658; AECL Research, Chalk River Laboratories: Chalk River, Ontario, Canada, 1996.

(22) Jou, F.-Y.; Freeman, G. R. *Can. J. Chem.* **1979**, *57*, 591.

(23) Lenchenkov, V. A.; Chen, X.; Vilchiz, V. H.; Bradforth, S. E. *Chem. Phys. Lett.* **2001**, *342*, 277. Lenchenkov, V. A. *Femtosecond Dynamics of Electron Photodetachment from Coordinated Anions*: *Hexaferrocyanate and Tribromocuprate in Solution*; University of Southern California: Los Angeles, CA, 2002.

(24) Shirom, M.; Stein, G. *J. Chem. Phys.* **1971**, *55*, 3372.

(25) Cohen; S. R.; Plane, R. A. *J. Phys. Chem.* **1957**, *61*, 1096. Davies, C. W. *J. Am. Chem. Soc.* **1937**, *59*, 1760.

(26) Perrin, D. D. *Ionization Constants of Inorganic Acids and Bases in Aqueous Solution*; Pergamon: Oxford, U.K., 1982.

(27) Rabinovitch, E. *Rev. Mod. Phys.* **1942**, *14*, 112.

(28) Elliot, A. J.; Sopchyshyn, F. C. *Int. J. Chem. Kinet.* **1984**, *16*, 1247. Jayson, G. G.; Parsons, B. J.; Swallow, A. J. *J. Chem. Soc., Faraday Trans.* **1973**, *69*, 1597. Zehavi, D.; Rabani, J. *J. Phys. Chem.* **1972**, *76*, 312. Devonshire, R.; Weiss, J. J. *J. Phys. Chem.* **1968**, *72*, 3815. Elliot, A. J. *Can. J. Chem.* **1992**, *70*, 1658. Schwartz, H. A.; Bielski, H. J. *J. Phys. Chem.* **1986**, *90*, 1445. Nagarajan, V.; Fessenden, R. W. *J. Phys. Chem.* **1985**, *89*, 2330.

(29) Karmann, W.; Meissner, G.; Henglein, A. *Z. Naturforsch. B* **1967**, *22*, 273.

(30) Fox, M. F.; Barker, B. E.; Hayon, E. *J. Chem. Soc., Faraday. Trans. 1* **1978**, *74*, 1777. Fox, M. F.; Hayon, E. *J. Chem. Soc., Faraday. Trans. 1* **1977**, *73*, 872.

(31) Fox, M. F.; Hayon, E. *J. Chem. Soc., Faraday Trans. 1* **1977**, *73*, 1003. Jortner, J.; Treinin, A. *Trans. Faraday Soc.* **1962**, *58*, 1503. Jortner, J.; Raz, B.; Stein, G. *Trans. Faraday Soc.* **1960**, *56*, 1273. Stein, G.; Treinin, A. *Trans. Faraday. Soc.* **1959**, *55*, 1091.

(32) Fox, M. F.; Hayon, E. *J. Chem. Soc., Faraday Trans. 1* **1979**, *75*, 1380.

(33) Shushin, A. I. *J. Chem. Phys.* **1992**, *97*, 1954; *Chem. Phys. Lett.* **1985**, *118*, 197, *J. Chem. Phys.* **1991**, *95*, 3657.

(34) Takahashi, N.; Sakai, K.; Tanida, H.; Watanabe, I. *Chem. Phys. Lett.* **1995**, *246*, 183 and references therein.